ELSEVIER

Journal of Alloys and Compounds 303–304 (2000) 245–251

Journal of ALLOYS AND COMPOUNDS

www.elsevier.com/locate/jallcom

Disorder and correlations in extended superconducting nanostructures

Daniel H. Reich[a,*], Daniel M. Silevitch[a], C.L. Chien[a], Dragomir Davidovic′[b], S.B. Field[c]

[a]*Department of Physics and Astronomy, The Johns Hopkins University, Baltimore, MD 21218, USA*
[b]*Department of Physics, Harvard University, Cambridge, MA 02138, USA*
[c]*Department of Physics, Colorado State University, Fort Collins, CO 80523, USA*

Abstract

Experiments are presented on the magnetic properties of two types of extended superconducting nanostructures where disorder can be introduced in a controlled way. Magnetotransport measurements on Nb films overlaying arrays of 250-nm diameter Ni dots show that the superstructure observed at higher multiples of the matching field $H_0 = \Phi_0/a^2$, where $a = 560$ nm is the dot lattice constant, are systematically suppressed as disorder is introduced into the dot arrays. In arrays of superconducting rings in external fields corresponding to half-integral numbers of flux quanta per ring, flux quanta trapped in individual rings repel each other due to the magnetic coupling between rings, and the system is analogous to an Ising antiferromagnet. Disorder enters through small, random variations in ring sizes, and plays the role of a random field in the Ising model. SQUID magnetometry and scanning Hall microscopy (SHM) were used to probe the dynamics and specific magnetic configuration of square, honeycomb, kagomé, and triangular lattice arrays containing up to 10^6 micron-size Al rings. The dynamics are dominated by a temperature-dependent energy barrier E_B and hysteresis in the flux state of the ring populations. This population hysteresis is directly observed in $\partial M/\partial T$ measurements. SHM measurements at $\Phi_0/2$ per ring show antiferromagnetic correlations that can be suppressed by going to higher flux fractions due to increases in the effective random field.

Keywords: Superconductors; Nanostructures; Order–disorder effects

1. Introduction

Superconducting nanostructures can now be produced that cover large areas with regular structures with sub-micron feature sizes. In an applied magnetic field, the interactions of magnetic flux vortices with these structures produces a variety of intriguing and unusual effects which can be tailored by varying the geometry of the device. There is now an extensive literature detailing with studies of Josephson junction arrays and superconducting wire networks. More recently, there have been a series of experiments on arrays of small holes, or 'anti-dots,' in superconducting films [1–3], sub-micron magnetic dots underlying superconducting films [4–6], and arrays of magnetically interacting superconducting rings [7,8]. Most experiments to date have focused on the novel properties that the high degree of order attainable through the lithographic fabrication process brings to the behavior of these systems. However, this same control over the system also makes this class of structures a good environment in which to study the effects of disorder [9]. In this paper, we present experiments on two examples of structures in which the effects of the interplay between lattice geometry and tunable, quenched disorder on an interacting many-body system can be studied in a controlled way.

The systems we will discuss are superconductor/magnetic dot arrays, and arrays of superconducting rings. In the former, the vortex lattice in a type-II superconductor is pinned by the presence of an underlayer of sub-micron magnetic dots, leading to enhanced transport properties when the flux lattice is commensurate with the dot lattice [4–6]. In ordered arrays, the flux lattice distorts to match the dot array, but, as we shall show, small amounts of disorder in the dot lattice rapidly eliminate the commensuration effects. In arrays of superconducting rings, at external magnetic fields corresponding to half-integral numbers of flux quanta per ring, flux quanta trapped in individual rings repel each other due to the magnetic coupling between rings, and the system is analogous to an Ising antiferromagnet. Differing degrees of correlation in the positions of the flux quanta can be seen for different array geometries, and effects of geometrical frustration can

*Corresponding author.

0925-8388/00/$ – see front matter
PII: S0925-8388(00)00667-8

be observed. Disorder enters through small, random variations in the rings' sizes, and plays the role of a random field in the Ising model. The strength of this random field can be tuned by working at different flux fractions, and can change dramatically the degree of correlation observed.

2. Superconductor/magnetic dot arrays

Along with the anti-dot arrays, ordered superconductor/magnetic dot (SC/MD) arrays fall into a class of systems whose behavior is determined by collective motion of the superconducting vortex lattice in the presence of periodic pinning [10,11]. The main effect of introducing periodic pinning into a superconducting film is a stabilization of the vortex lattice at integral multiples of the so-called 'matching field' $H_0 = \Phi_0/a^2$, where Φ_0 is the superconducting fluxoid quantum, and a^2 is the area per pinning site. To date, only transport studies of the SC/MD systems have been reported, where reductions in the flux-flow resistance [4,5] and enhancements of the critical current [6] at multiples of H_0 are found.

By perturbing the system away from this ordered limit, we may study the stability of the novel effects produced by that order. More generally, the problem of collective motion in a disordered or partially ordered medium may ultimately be addressed. Here we will discuss results on the effects of introducing controlled randomness in the positions of an array of Ni dots underlying a Nb thin film.

Our Ni dot arrays were made by electron beam lithography, thermal evaporation, and lift-off. The positions of the dot are randomized by perturbing their positions about an ideal square lattice with lattice constant $a = 560$ nm. A flat random distribution was used to vary the positions up to a cutoff δa, which was varied between zero and $0.4a$. The dots had diameter 250 nm, and were written over 35×35 μm^2 fields. A Nb film was then sputtered on top, and patterned for four-lead transport measurements.

Fig. 1(a) shows the magnetoresistance at several fixed temperatures T near the bottom of the zero-field resistive transition for a Nb film overlaying an array of ordered dots. We see sharp dips in the resistance of the array at integral multiples $H_n = nH_0$ ($H_0 = 65$ G here), as has been reported previously [4,5]. These dips become larger with decreasing T, and the higher-order dips increase in prominence. In addition, we observe features at half-integral multiples of H_0, most prominently at $0.5H_0$. Fig. 1(b) shows the magnetoresistance of an array where the dot positions have been randomized in the direction parallel to the measuring current with $\delta a = 0.2a$. The main dips at $\pm H_0$ are broadened, and those at higher multiples of H_0 are suppressed or eliminated. No evidence for the half-integral features is observed.

These results are representative of measurements made on a number of samples with varying disorder. The higher integral matching field features are progressively destroyed

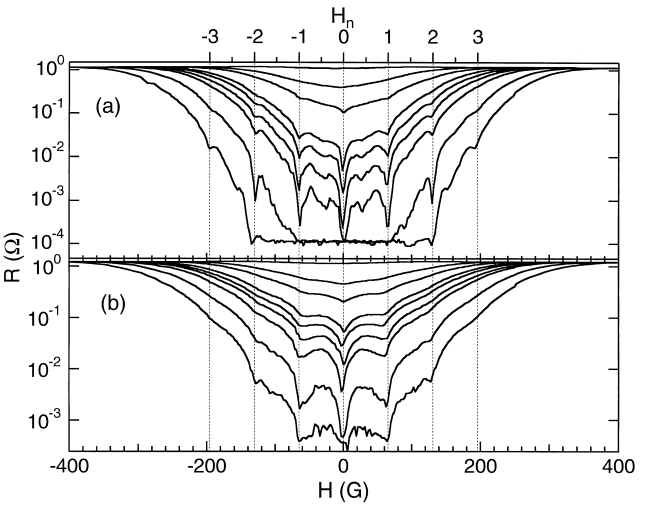

Fig. 1. Magnetoresistance of Nb-films overlaying (a) ordered and (b) 20% disordered arrays of magnetic Ni dots. In both (a) and (b) from bottom to top, the traces are at $T = 8.37$, 8.38, 8.39, 8.395, 8.40, 8.41, 8.42, 8.43, and 8.46 K. The first matching field is at $H = 65$ G.

with increasing randomness, but the broadened $n = 1$ feature remains for δa as large as $0.4a$, by which point all vestiges of short-range order in the dot arrays is gone. Further details of these results will be given in a future publication [12].

Thus these results demonstrate that in these arrays, we have a clean model system for the exploration of the effects of the systematic introduction of randomness on collective motion and dynamic critical phenomena. Lorenz microscopy imaging experiments on ordered antidot arrays [1] have shown that for $n > 1$ in the static limit ordered configurations with some vortices on the antidots, and some at high symmetry interstitials are stable. The transport measurements on ordered arrays suggests that even in a moving lattice some vestige of this stable state remains. It should be possible in the future to correlate our transport results on disordered systems with imaging experiments to determine in detail the mechanism by which the ordered states and collective pinning are destroyed.

3. Arrays of superconducting rings

Unlike the other systems we have mentioned, the superconducting ring arrays are unique in that the individual elements of the array are electrically isolated from each other, and only couple magnetically when a persistant current in one ring produces a magnetic field felt by its neighbors. In an applied flux near $\Phi_0/2$, a superconducting ring has two states containing $n = 0$ and $n = 1$ fluxoid quanta, respectively, that are close in energy. Exactly at $\Phi_0/2$ these states are energetically degenerate, but with oppositely circulating currents induced to maintain fluxoid quantization. The magnetic moment of the ring can thus point either up or down, and the ring may be thought of as

an Ising spin. Two such neighboring rings are coupled 'antiferromagnetically' in that the field produced by a spin-down ring ($n=0$) adds to the applied field on its neighbor, biasing that ring into the spin-up ($n=1$) state. That rings field opposes the applied field at the site of the first ring, stabilizing the first ring in the $n=0$ state. This effect may also be seen as a repulsive interaction between flux quanta.

By exploiting our ability to tailor these 'spin systems' lithographically, we have been able to address important questions in magnetism regarding the role of lattice geometry and geometrical frustration on antiferromagnetic (AFM) correlations, using a combination of SQUID magnetometry and scanning Hall probe microscopy. Here we will briefly review some of our main previous results [7,8], and will present new results that address two of the crucial aspects of these ring arrays: the spin-freezing that dominates the dynamics of the individual rings, and the role played by residual disorder. This disorder, arising from variations in the rings' sizes, produces a distribution of fields for $\Phi_0/2$, and acts like a tunable random field in the Ising model.

Arrays containing up to 10^6 aluminum rings were fabricated on insulating substrates at the Cornell Nanofabrication Facility using electron beam lithography, e-beam evaporation, and lift-off. Examples of these arrays are shown in Fig. 2. The main arrays are the four on the left, containing square rings 1.6 μm across on both dense and sparse (not shown) lattices, and similarly sized hexagonal rings on honeycomb, kagomé, and triangular lattices. Of these four, the first two are bipartite, and can support Néel order for Ising spins, while the latter two are non-bipartite, and cannot. We also studied larger, 3-μm square rings, as shown on the right of Fig. 2. While they are less well-optimized to study interaction effects than are the smaller, thicker rings [8], they are convenient for studies of ring dynamics at applied fluxes larger than $\Phi_0/2$.

3.1. Magnetic measurements

In this section we will describe measurements made with a special-purpose SQUID magnetometer [13] that explore the magnetic response of entire ring arrays. Inset (a) in Fig. 3 shows the average DC magnetic moment per ring μ at fixed field H vs. T near T_C for an array of the 3-μm rings shown in Fig. 2. If $H<1.34$ G, $\mu<0$ (antiparallel to H), indicating that the rings are in the $n=0$ 'spin down' state. If the $H>1.34$ G, $\mu>0$, and the rings are in the $n=1$ 'spin up' state. If $H\approx1.34$ G, $\mu\approx0$ because half of the rings have $n=0$ and half have $n=1$. Hence, $\bar{H}_{1/2}=1.34$ G is the average field for $\Phi_0/2$ per ring for this array. For the 1.6-μm square rings we find $\bar{H}_{1/2}=7.53$ G, and for the hexagonal rings $\bar{H}_{1/2}=6.98$ G. The figure also shows that near $T_C(\Phi_0/2)$, μ, and thus the

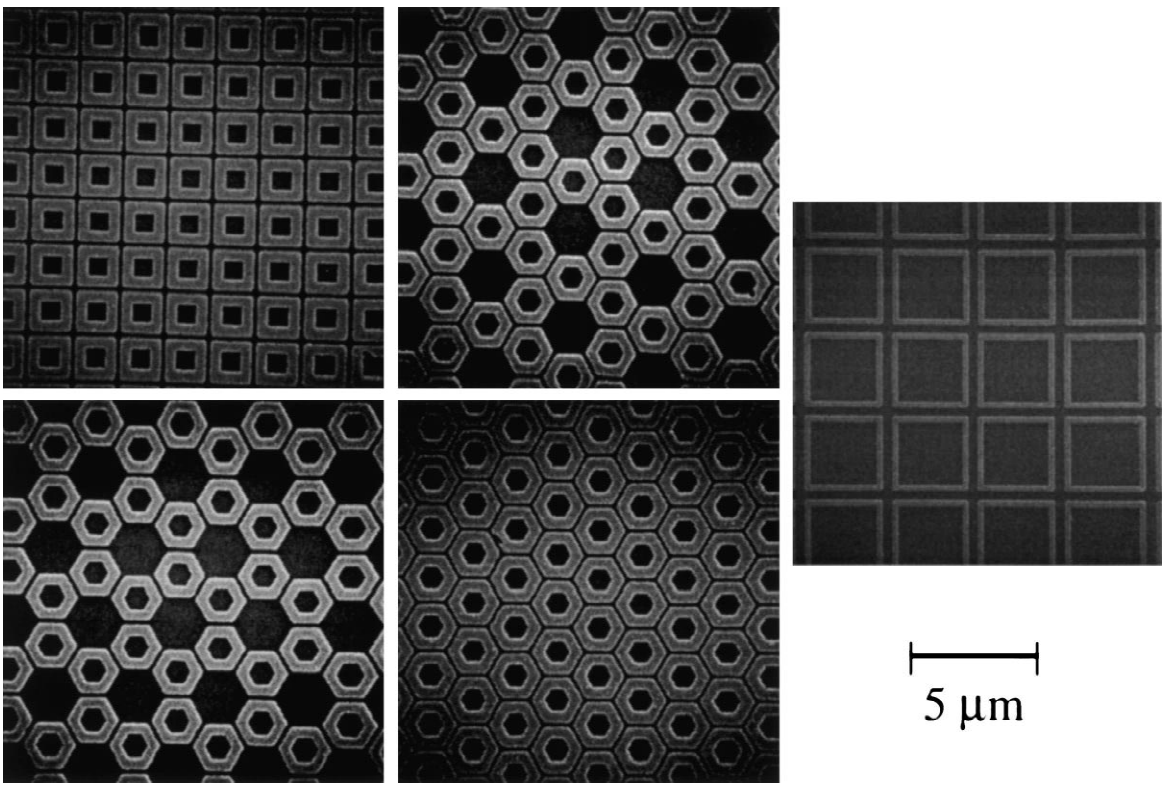

Fig. 2. SEM images of portions of arrays of Al rings. Small squares and hexagons have 0.4-μm linewidth, and are 0.240-μm thick. Large squares have 0.2-μm linewidth, and are 0.12-μm thick.

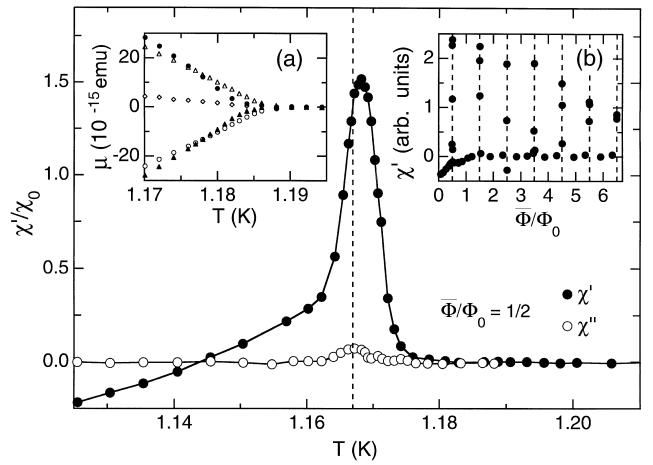

Fig. 3. Ac susceptibility, χ, of an array of 1.6-μm square rings T_C in a DC flux of $\Phi_0/2$. The large paramagnetic spike in χ' appears as the rings flip in response to the ac field. The freezing temperature T_f (dashed line) is defined by the peak in χ'' (triangles). The data are normalized to χ_0, the value of χ at low T. Inset (a): Magnetic moment per ring vs. temperature for an array of 3-μm square Al rings. Solid triangles: $H=0.964$ G; open circles: $H=1.269$ G; open diamonds: $H=1.343$ G; solid circles: $H=1.365$ G; open triangles: $H=1.694$ G. Inset (b): χ' at higher fractions of $\Phi_0/2$, for the 3-μm square rings, at $T=1.178$ K. Dashed lines indicate $(n+1/2)\Phi_0$.

current flowing in each ring, is linear in T. Extrapolating $\mu(T)$ to zero yields the Ginzburg–Landau $T_C(H)$, which may be seen to have a minimum at $\bar{H}_{1/2}$, which is the Little–Parks effect [14].

Measuring the ac susceptibility $\chi(H,T)$ probes rings' dynamics directly. The main part of Fig. 3 shows the real and imaginary part of the susceptibility $\chi^{\pm}$ and $\chi^{\pm\prime\prime}$ for a dense array of 1.6-μm square rings measured with a 6 mG ac field at frequency $f=3$ Hz in an average applied DC flux $\bar{\Phi}=0.5\ \Phi_0$. Φ is defined such that $\Phi=\Phi_0/2$ when $H=\bar{H}_{1/2}$ magnetization or SHM measurement. There is a dramatic paramagnetic spike in χ' just below T_C as the rings switch between the $n=0$ and $n=1$ fluxoid states in response to the ac field, just as for spins in a magnetic system. This flipping between states can be seen at higher fields as well. Inset (b) in Fig. 3 shows susceptibility vs. field for for the 3-μm square rings at a few mK below T_C. We see a repetition of the paramagnetic spikes at higher half-integral fractions $\nu=\bar{\Phi}/\Phi_0$.

This peak in $\chi(T)$ is a single-ring effect that we observe in all arrays, irrespective of ring size or separation. A similar feature has also been observed in experiments on individual Al rings [15]. The behavior of this peak is determined by the rings' dynamics, which are those of a two-level system with a strongly temperature-dependent energy barrier $E_B \sim[1-T/T_c\ (\Phi_0/2)]^2$ [8]. As with any spin system, the ac response freezes out when the relaxation rate $\Gamma=\Omega e-E_B/k_BT$ becomes less than the measuring frequency. The accompanying peak in χ'' shown in Fig. 3 defines the (frequency-dependent) average freezing temperature T_f. Below T_f the continued increase of E_B prohibits further spin flipping, and thus there is only a narrow range of temperature between T_c and T_f where cooperative phenomena can influence the behavior of the ring arrays. Ref. [8] gives a quantitative analysis of these effects in terms of a disorder-induced distribution in relaxation rates.

The presence of magnetic interactions between rings in the arrays can be observed in measurements of the field-dependence of the susceptibility $\chi(H)$ at fixed T near the peak in $\chi(T)$. Fig. 4 shows the response of a dense honeycomb array above and below the temperature T_p of the peak in $\chi(T)$. Data taken for both increasing and decreasing H are shown. The shapes of these peaks are well-described by Gaussians, as shown by the solid curves. The dominant source of their width is the effective random field arising from variations in the rings' sizes which leads to a spread in fields $H_{1/2}$ needed to produce $\Phi_0/2$ on different rings in the array. This is seen in both dense and sparse arrays [8].

In the dense arrays, the interactions broaden the peak both above and below T_P, and shift the peaks to lower or higher field upon sweeping H up or down, respectively. For example, when starting a field sweep at low fields, almost all of the rings will point down. Since a spin-down ring produces a magnetic field pointing *up* on its neighbors, the actual field H_a felt by the rings is initially *larger* than H. The largest rings in the distribution will therefore reach their flipping field $H_{1/2}$ at a lower applied field than they would have without interactions, and χ will begin to rise sooner. The effect is reversed above $\bar{\Phi}=\Phi_0/2$ where more spins are up, and a larger field is needed to produce $H_{1/2}$ for the smallest rings than without interactions.

The splitting below T_p is caused by a distribution in the barriers E_B that are beginning to freeze out the rings. Some rings that have stopped responding to the ac field still have E_B small enough so that they can be flipped once from

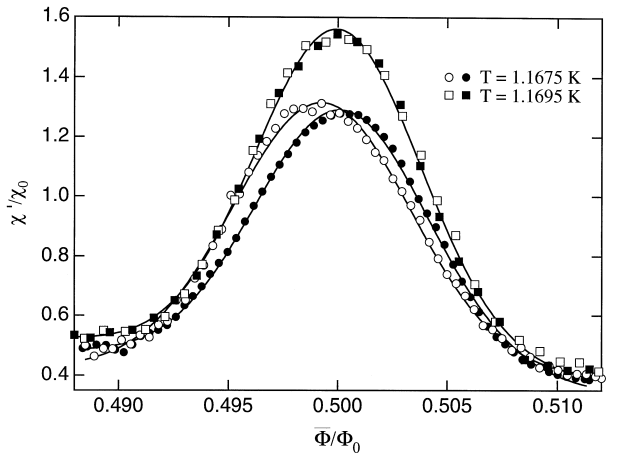

Fig. 4. Field-dependence of the ac susceptibility of interacting rings on a honeycomb lattice for T above (squares) and below (circles) the peak in χ(T). Open symbols: increasing field; filled symbols: decreasing field. Solid lines are fits to Gaussians.

down to up as the DC field is increased. Hysteresis in the population of these rings produces hysteresis in interaction field felt by those rings that are still contributing to χ, causing the peak in the upward (downward) sweeps to occur below (above) $\bar{\Phi} = \Phi_0/2$.

This hysteresis in the ring population can be observed directly by measuring the temperature-derivative of the magnetization $\partial M/\partial T$. In $\partial M/\partial T$ measurements [16], the temperature of the sample is modulated, leading to a modulation of the superconducting order parameter of the rings. This gives a time-dependent magnetization which can be detected by the SQUID. The inset of Fig. 5 shows $\partial M/\partial T$ vs. T for a dense 1.6-μm square ring array. The lower curve shows $\partial M/\partial T$ when $\bar{\Phi} < \Phi_0/2$, so that all the rings cooled into the diamagnetic, $n=0$ state. The upper curve shows $\partial M/\partial T$ for $\bar{\Phi} > \Phi_0/2$, where all the rings cool in the paramagnetic, $n=1$ state. The middle curve was obtained at $\bar{\Phi} \approx \Phi_0/2$.

Now we turn to field scans at temperatures near T_C. As the applied flux varies, the occupancy of the $n=0$ and $n=1$ states in the array changes and $\partial M/\partial T$ changes from its $n=0$ state value $dM_\downarrow/dT < 0$ to its $n=1$ state value $dM_\uparrow/dT > 0$. Fig. 5 shows field scans for $T > T_P$ where thermal fluctuations are strong. The main qualitative difference between the two curves is that the lower temperature curve saturates near the two ends of the field sweep because at this T the sample is at the low temperature end of the fluctuation region, where $\partial M/\partial T$ becomes independent of temperature. Fig. 6 shows that hysteresis develops at lower T. As T decreases, the total number of rings that flip between the two states in the field sweep gets smaller, and rings that do flip between the two states lag behind the applied field, i.e. the flux needed to make them flip is getting further away from $\Phi_0/2$ and the splitting between the up and down curves increases. It is this hysteresis that produces the shift in the peaks of $\chi(H)$ described above.

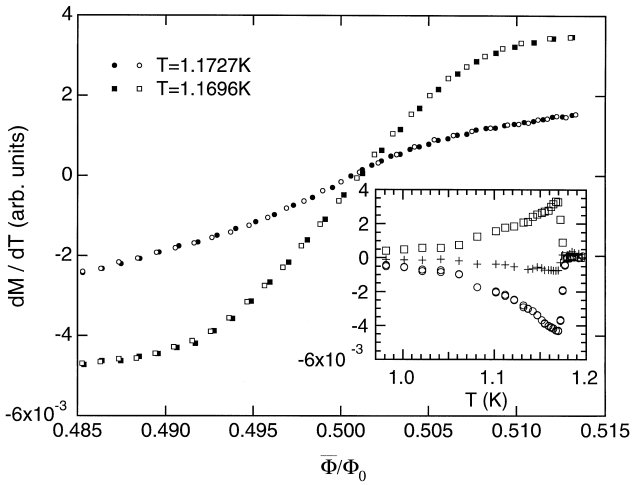

Fig. 5. $\partial M/\partial T$ vs. H for an array of 1.6-μm square rings, at temperatures above T_P. Filled symbols: increasing H. Open symbols: decreasing H. Inset: temperature dependence of $\partial M/\partial T$ at $0.48\Phi_0$ (circles), $0.5\Phi_0$ (crosses), and $0.52\Phi_0$ (squares).

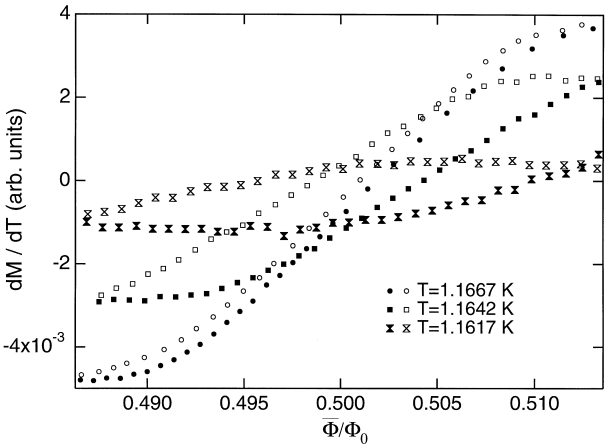

Fig. 6. $\partial M/\partial T$ vs. H at temperatures below T_P for an array of 1.6-μm square rings. Filled symbols: increasing H. Open symbols: decreasing H.

3.2. Magnetic imaging

To study directly the magnetic correlations in the ring arrays implied by the susceptibility measurements, we used a scanning Hall probe microscope (SHM) [17–19] to map specific magnetic configurations in the arrays. These images were recorded at $T \approx 0.6\ T_C$ after field-cooling the arrays from above T_C. Hence they are images of the spin configurations frozen in near T_P.

Three examples of the magnetic field maps of the ring arrays are shown in Fig. 7. These were taken at different applied fields over the same $50 \times 60\ \mu m^2$ area of a honeycomb array, which contains approximately 680 rings. The full-scale field modulation in these pictures is 0.53 G, and lighter colors correspond to larger field. For $\bar{\Phi} < \Phi_0/2$ the rings in the up state appear as white spots against the dark background of the majority down rings. For $\bar{\Phi} > \Phi_0/2$ the situation is reversed, and the minority down rings appear as dark spots against the white up-ring background. At $\bar{\Phi} = \Phi_0/2$ there are equal numbers of up and down rings.

The lower panels in Fig. 7 show the spin configurations as deduced from analysis of the corresponding images. Despite the obvious absence of Néel-type checkerboard ordering in these configurations, the location of the up and down spins are not random; there are measurable short-range antiferromagnetic correlations. One measure of this is the bond order parameter [20]

$$\sigma = 1 - \frac{n_{AF}}{2x_+x_-} \quad (1)$$

where n_{AF} is the fraction of antiferromagnetic bonds, and x_+ and x_- are the concentrations of up and down spins, respectively. σ ranges from $+1$ for a ferromagnet through

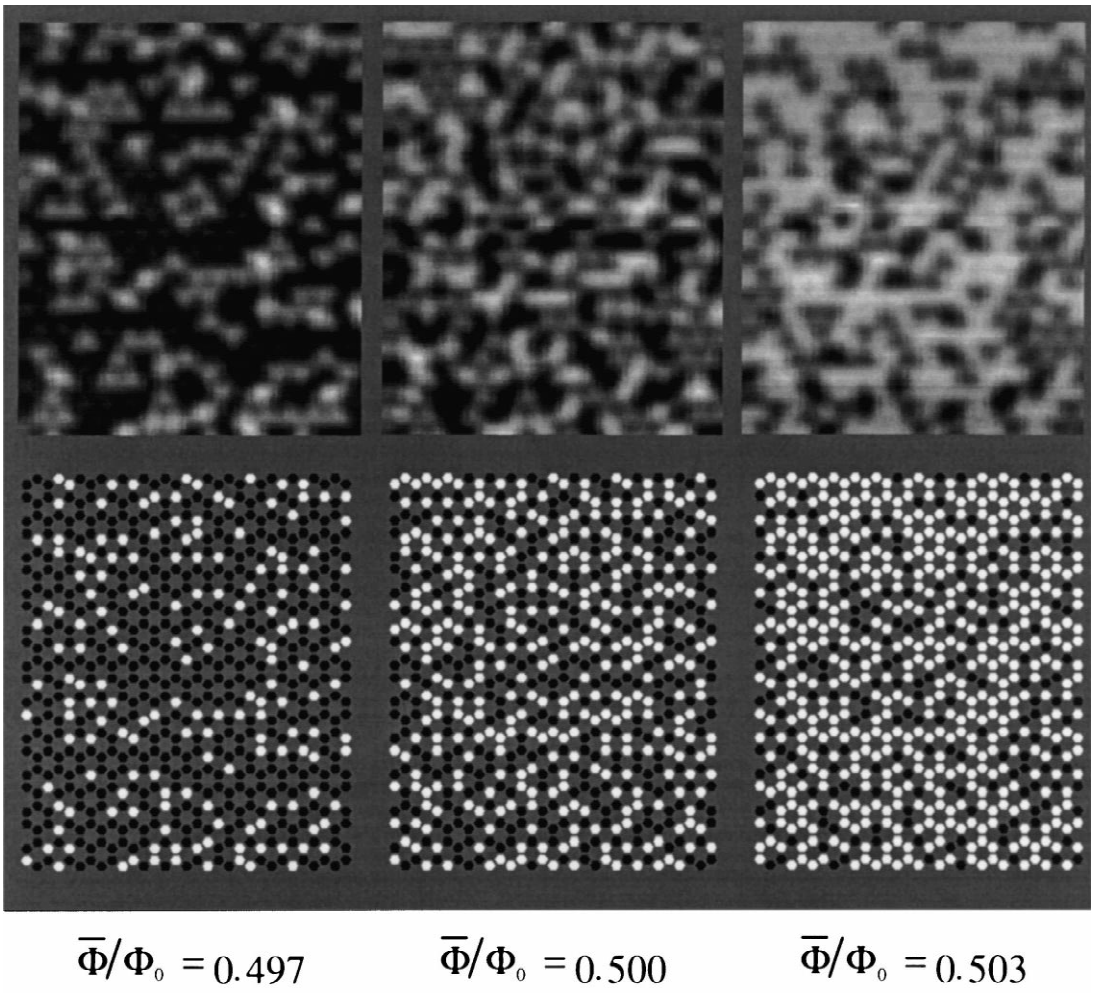

Fig. 7. Top row: magnetic field above a honeycomb ring array as measured by the scanning Hall probe microscope. 'Up' spins appear as white spots, and 'down' spins as black ones. Bottom row: spin configurations as deduced from the images. White hexagons are up spins; black hexagons are down spins.

zero for a random configuration to -1 for a Néel-ordered antiferromagnet at $x_+ = 1/2$.

To assess the effects of lattice geometry, Fig. 8 shows σ vs. x_+ measured for series of images near $\bar{\Phi} = \Phi_0/2$ for the three hexagonal ring arrays. Each point in this figure corresponds to a scan such as those in Fig. 7. Although there is scatter in the data, the antiferromagnetic correlations are visibly stronger in the bipartite honeycomb array than for the non-bipartite kagomé and triangular arrays. This is thus direct experimental evidence for geometrical frustration in this system.

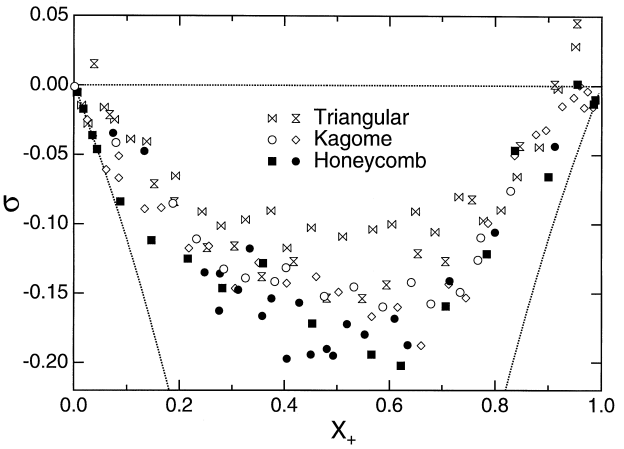

Fig. 8. Bond order parameter, σ, vs. concentration of up spins x_+ at $\bar{\Phi} = \Phi_0/2$ for the honeycomb, kagomé, and triangular lattice arrays. Slanted dashed lines indicate theoretical limits of σ.

The growth of antiferromagnetic correlations in the bipartite lattices is limited by the effective random field produced by the variation in ring sizes in combination with the spin freezing. At low temperatures, the magnetic interactions between rings are easily strong enough to overcome the random field, and induce measurable longer range correlations. However, as their ability to find their ground state is cut off by the spin-freezing at T_f, the arrays as they are imaged remain frozen in a metastable state that reflects the correlations present at T_f.

Interestingly enough, it is possible to change the strength of the random field by going to higher half-integral flux fractions ν where, as shown above, the rings

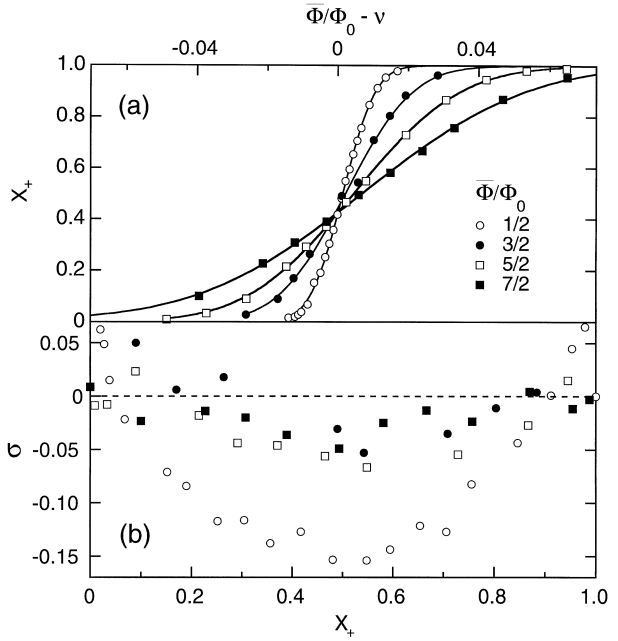

Fig. 9. Effects on a triangular lattice array of the growth of the random field with increasing flux fraction ν. (a) Up spin concentration x_+ vs. field at different ν. Inset: width determined from Gaussian fits (solid lines). (b) Bond order parameter σ vs. ν at different ν.

retain their Ising spin character. The random field, however, increases with ν because it is caused by the differences in the ring areas. The field for ν flux quanta in a ring with area A is $H_\nu = \nu\Phi_0/A$. If the spread of the areas in the array is δA, and if it is small, then we can estimate the spread in fields $\delta H_\nu = \nu\Phi_0\delta A/A^2$. This can be seen in Fig. 9(a), which shows the up-spin concentration x_+ vs. flux in a triangular lattice array for images taken around various flux fractions. The broadening of these curves with increasing ν shows that the random field indeed grows. The width of these curves as determined from fits to integrals of a Gaussian distribution (error functions) is shown in the inset to Fig. 9(a). It is linear with ν as one would expect from the argument given above. If the disorder increases with ν, then the antiferromagnetic correlations should decrease. This is indeed the case, as is shown for the triangular lattice in Fig. 9(b). Thus disorder is a tunable parameter in these superconducting ring arrays.

4. Summary

The experiments presented here show some of the unique possibilities for exploration of novel phenomena that arrays of extended superconducting nanostructures present. The example of the superconducting ring arrays shows that the combination of bulk measurements that are sensitive to dynamics with real-space imaging provided by scanned probe microscopy techniques can yield enormously detailed pictures of the behavior of these artificially structured systems. The SC/MD arrays show promise for the study of collective dynamic phenomena under the influence of randomness and periodic disorder. Coupled with the ability to tailor the properties of the individual elements of the arrays through lithography, it is thus now possible to make quantitative studies of a variety of model systems that can potentially shed light on very general problems in condensed matter physics.

Acknowledgements

It is a pleasure to acknowledge the contributions of S. Kumar, J. Siegel, and R. Tiberio to some of the work reported here. Work at JHU was supported by NSF grants DMR 93-57518 and DMR 96-32526, and by the David and Lucile Packard Foundation. The work was performed in part at the Cornell Nanofabrication Facility which is supported by the NSF under Grant ECS-8619049, Cornell University and industrial affiliates.

References

[1] K. Harada et al., Science 274 (1996) 1167.
[2] V.V. Moshchalkov et al., Phys. Rev. B 57 (1998) 3615.
[3] B. Pannetier, A. Bezryadin, A. Eichenberger, Physica B 222 (1996) 253.
[4] J.I. Martin et al., Phys. Rev. Lett. 79 (1997) 1929.
[5] Y. Jaccard et al., Phys. Rev. B 58 (1998) 8232.
[6] D.J. Morgan, J. Ketterson, Phys. Rev. Lett. 80 (1998) 3614.
[7] D. Davidovic′ et al., Phys. Rev. Lett. 76 (1996) 815.
[8] D. Davidovic′ et al., Phys. Rev. B 55 (1997) 6518.
[9] M.A. Itzler et al., Phys. Rev. B 42 (1990) 8319.
[10] C. Reichhardt, C.J. Olson, F. Nori, Phys. Rev. B 57 (1998) 7937.
[11] C.J. Olson, C. Reichhardt, F. Nori, Phys. Rev. Lett 81 (1998) 3757.
[12] D.M. Silevitch, D.H. Reich, C.L. Chien, unpublished.
[13] D. Davidovic′, Ph.D. Thesis, The Johns Hopkins University, 1996.
[14] W.A. Little, R.D. Parks, Phys. Rev. Lett. 9 (1962) 9.
[15] X. Zhang, J.C. Price, Phys. Rev. B 55 (1997) 3128.
[16] P. Gandit et al., Europhys. Lett. 3 (1987) 623.
[17] J. Siegel et al., Rev. Sci. Instrum. 66 (1995) 2520.
[18] A.M. Chang et al., Appl. Phys. Lett. 61 (1992) 1974.
[19] H.D. Hallen et al., Phys. Rev. Lett. 71 (1993) 3007.
[20] J.M. Cowley, Phys. Rev. 77 (1950) 669.